Unambiguous identification of N-containing oxygenated organic moleculesusing a chemical-ionization Orbitrap (CI-Orbitrap) in an eastern Chinese megacity

Y. Lu, Y. Ma, D. Huang, S. Lou, S. Jing, Y. Gao, H. Wang, Y. Zhang, H. Chen, Y. Chang, et al.

Atmos. Chem. Phys., 23, 3233–3245, 2023
https://doi.org/10.5194/acp-23-3233-2023

Atmospheric Chemistry and Physics
Open Access
EGU

Unambiguous identification of N-containing oxygenated organic molecules using a chemical-ionization Orbitrap (CI-Orbitrap) in an eastern Chinese megacity

Yiqun Lu[1,2], Yingge Ma[1], Dan Dan Huang[1], Shengrong Lou[1], Sheng'ao Jing[1], Yaqin Gao[1], Hongli Wang[1], Yanjun Zhang[3], Hui Chen[4], Yunhua Chang[5], Naiqiang Yan[2], Jianmin Chen[4], Christian George[3], Matthieu Riva[3], and Cheng Huang[1]

[1]State Environmental Protection Key Laboratory of Formation and Prevention of Urban Air Pollution Complex, Shanghai Academy of Environmental Sciences, Shanghai 200233, China
[2]School of Environmental Science and Engineering, Shanghai Jiao Tong University, Shanghai 200240, China
[3]Univ. Lyon, Université Claude Bernard Lyon 1, CNRS, IRCELYON, 69626 Villeurbanne, France
[4]Shanghai Key Laboratory of Atmospheric Particle Pollution and Prevention (LAP[3]), Department of Environmental Science and Engineering, Jiangwan Campus, Fudan University, Shanghai 200438, China
[5]Collaborative Innovation Center on Forecast and Evaluation of Meteorological Disasters (CIC-FEMD), NUIST Center on Atmospheric Environment, Nanjing University of Information Science and Technology, Nanjing 210044, China

Correspondence: Cheng Huang (huangc@saes.sh.cn)

Received: 13 November 2022 – Discussion started: 17 November 2022
Revised: 13 January 2023 – Accepted: 23 February 2023 – Published: 13 March 2023

Abstract. Oxygenated organic molecules (OOMs) are dominated by the N-containing species in polluted urban environments. As N-containing OOMs, especially those with more than one nitrogen atom, prevail in the high m/z (mass-to-charge) range ($m/z > 350$ Th), unambiguous identification of N-containing OOMs is highly desirable for understanding of their formation processes, precursors and influencing factors. To achieve this, we applied an ultra-high-resolution chemical-ionization Orbitrap (CI-Orbitrap) in a field campaign and found that OOMs contain one (1N-OOMs), two (2N-OOMs) and three (3N-OOMs) nitrogen atoms comprised 50 %, 26 % and 4 %, respectively, of total OOMs. More interestingly, the fraction of 2N-OOMs increased with the increase in carbon number (nC) and was dominated by the ones derived from aliphatic precursors (2N-OOM_{Ali}, 64.2 %), indicating the importance of multistep oxidation. Plausible precursors of 2N-OOMs were aliphatics (2N-OOM_{Ali}, 64.2 %), aromatics (2N-OOM_{Aro}, 16 %) and monoterpenes (2N-OOM_{MT}, 15.4 %). The absolute concentrations of 2N-OOMs were greatly affected by the pollution level for most cases. The 2N-OOM_{Ali} was the most abundant 2N-OOM, and its fraction even increased on the polluted day with an enhanced proportion of the ones with nC > 10. While 2N-OOM_{Ali} and 2N-OOM_{Aro} were dominated by daytime photochemical production, nighttime NO_3-initiated oxidation played a comparable role to the daytime photochemistry in the formation of 2N-OOM_{MT}. The 2N-OOM_{Aro} species were of the highest oxygenation level, followed by 2N-OOM_{MT} and 2N-OOM_{Ali}, which were affected by photochemistry and NO_x concentrations. These results highlight the significant formation of 2N-OOMs and the influencing factors on their formation in polluted urban environments, where various volatile organic compound (VOC) precursors and atmospheric oxidants are present.

Published by Copernicus Publications on behalf of the European Geosciences Union.

1 Introduction

Secondary organic aerosol (SOA) accounts for a significant fraction of particulate matters (Donahue et al., 2009; Ehn et al., 2014; Hallquist et al., 2009; Jimenez et al., 2009). Volatile organic compounds (VOCs) and their oxidation products, i.e., OVOCs, are important precursors of SOA in the atmosphere (Atkinson and Arey, 2003; Bianchi et al., 2019; Ehn et al., 2014; Nie et al., 2022). N-containing oxygenated organic molecules (OOMs) have been identified as important products upon VOC oxidation. Especially at high NO_x levels, these products become more dominant, while the others (i.e., alcohols, hydroperoxides and RO_2 cross-reaction products) are likely suppressed (Bianchi et al., 2019; Zhao et al., 2018). The nitrogen atoms in OOMs are assumed to be mainly associated with the nitrate group ($-ONO_2$) formed from bimolecular reaction between RO_2 radical and NO. Field measurements have also shown that up to 77 % of molecules in organic aerosol (OA) contain nitrate functional groups under different atmospheric conditions (Ditto et al., 2020; Kenagy et al., 2021; Kiendler-Scharr et al., 2016; Lee et al., 2016; Ng et al., 2017; Lin et al., 2021; Rollins et al., 2013; Xu et al., 2015; Ye et al., 2021; Yu et al., 2019).

The N-containing OOMs can be classified into 1N-OOMs, 2N-OOMs and 3N-OOMs, according to the number of N atoms in the molecule. The chemical composition of N-containing OOMs is determined by their precursors, formation pathways and NO_x level in the atmosphere (Bianchi et al., 2019; Ehn et al., 2014; Nie et al., 2022; Pye et al., 2019; Riva, 2016; Yan et al., 2016). Recent observations in megacities of China have indicated that 2N-OOMs account for significant fractions (about 30 %–33 %) among total N-containing OOMs besides 1N-OOMs (66 %–70 %) due to the high NO_x concentrations in polluted urban environments (Nie et al., 2022; Yan et al., 2021). Some laboratory studies have also proposed that the potential formation pathways of 2N-OOMs, such as multiple-step OH oxidation (Garmash et al., 2020) or NO_3-initiated oxidation followed by NO termination (Kiendler-Scharr et al., 2016; Liebmann et al., 2019), suggest the increased importance of multistep bimolecular oxidation in the formation of 2N-OOMs. On the other hand, it has also been found that the formation of 2N-OOMs shows a clear preference for specific precursors compared to 1N-OOMs, i.e., a significantly higher branch ratio of 2N-OOMs from aliphatic hydrocarbons compared to those from aromatics (Nie et al., 2022), suggesting a considerable difference from 1N-OOMs in terms of the formation pathway. Determining the formation pathway of N-containing OOMs, especially those containing two to three nitrogen atoms, in real atmosphere is challenging. Identification of their chemical compositions at the molecular level is key for advancing our understanding of the precursors, formation and sources of N-containing OOMs in polluted atmosphere, where thousands of oxidation products exist and evolve constantly.

Traditionally, a chemical-ionization atmospheric-pressure-interface time-of-flight mass spectrometer (CI-APi-TOF) has been used to measure gaseous OOMs (Berndt et al., 2016; Ehn et al., 2014; Jokinen et al., 2014; Rissanen et al., 2014). Using a CI-APi-TOF, an increasing number of studies have reported the formation of OOMs through the oxidation of various VOC precursors in chambers or flow tubes (Berndt et al., 2016, 2018; Ehn et al., 2014; Garmash et al., 2020; Jokinen et al., 2014, 2015; Rissanen et al., 2014; Wang et al., 2020; Zhao et al., 2018). While 2N-OOMs in real ambient atmosphere are almost exclusively located in a high m/z (mass-to-charge) range (i.e., 300–500 Th), a CI-APi-TOF with the highest mass resolving power of 12 000 ($m/\Delta m$, in full width at half maximum) at $m/z = 200$ Th and above can hardly identify the molecular compositions of 2N-OOMs unambiguously. This is because low mass resolving power imposes significant uncertainties onto separating overlapping peaks, which increase rapidly with increasing m/z and decreasing mass resolving power. Taking the integer m/z of 342 as an example, multiple peaks overlap at this nominal mass, i.e., $C_7H_8O_{10}N_2(NO_3)^-$ (342.0057 Th), $C_8H_{12}O_9N_2(NO_3)^-$ (342.0421 Th), $C_9H_{16}O_8N_2(NO_3)^-$ (342.0785 Th) and $C_{10}H_{20}O_7N_2(NO_3)^-$ (342.1149 Th). The adjacent peaks are of mass differences (m) of 0.0364, and a good peak separation of these peaks (4σ) requires mass resolving power of at least 16 000. Therefore, the development and application of mass spectrometry techniques with extremely high performance in terms of the detection limit, time resolution and mass resolving power are highly desirable.

To achieve accurate identification of the molecular formula from the extremely complex mass spectra, a CI (nitrate) inlet has also been coupled to an Orbitrap mass spectrometer (CI-Orbitrap) to measure the OOMs at ultra-high mass resolving power ($m/\Delta m > 100\,000$ at $m/z = 200$ to 500 Th) (Riva et al., 2019a; Zhang et al., 2022). The ultra-high mass resolving power of CI-Orbitrap will undoubtedly provide significant improvements in molecular identification, separation and quantification. Herein, we applied a CI-Orbitrap in a field campaign for the measurements of OOMs, with a special focus on 2N-OOMs, at the molecular level in urban Shanghai. The site represents a typical eastern Chinese megacity characterized by intense human activity, multiple anthropogenic emissions and high NO_x concentrations. Based on the measurement results as well as our current knowledge on N-containing OOM formation, we classify the observed 2N-OOMs into different precursor groups and explore the potential influencing factors in their formation. Furthermore, supported by positive matrix factorization (PMF), sources and gas-phase oxidation processes for 2N-OOM formation in urban Shanghai are identified.

2 Ambient measurement and methodology

2.1 Measurements

The field campaign was carried out from 31 October to 18 November 2020 on the top floor of an eight-story building in the Shanghai Academy of Environmental Sciences (31°18′ N, 121°43′ E; Fig. S1), which sits in a densely populated region surrounded by commercial properties and residential dwellings without significant industrial sources nearby. The site can represent a typical urban area of Shanghai affected by severe local emissions from vehicular traffic and commercial and residential activities. Our campaign was carried out in autumn, which represents a typical transition period from strong photochemistry in summer to intense regional transport in winter. At times, air masses transported from the neighboring provinces or even further from northern China can also affect the air quality of the site.

The 2N-OOMs as well other OOMs were measured in real time with a nitrate Orbitrap. The operation of the nitrate Orbitrap has been detailed in previous studies as well as in one of our companion studies (Zhang et al., 2022); thus it is only briefly described here. Ambient air was drawn into the ionization source through a 1 m stainless-steel tube (3/4 in.). The reagent ion was produced by passing nitric acid in sheath flow (20 L min^{-1}) into a Photoionizer (Model L9491, Hamamatsu, Japan) and was then introduced into a co-axial laminar flow reactor, in which the reagent ions interact with the air samples. The charged species were detected by an Orbitrap mass analyzer with a mass resolving power of about 140 000. Mass-dependent transmission calibrations were also performed using a depletion method (Heinritzi et al., 2016). Other ancillary measurements, including of the $PM_{2.5}$ concentrations, trace gases (SO_2, O_3 and NO_x) and volatile organic compounds, as well as meteorological parameters (wind direction and speed, solar radiation, etc.), are detailed in the Supplement (Sect. S1). An overview of the measurement data, illustrating the air quality as well as the meteorological conditions during the campaign, is provided in Sect. S2 and Fig. S2.

2.2 Data analysis of nitrate CI-Orbitrap

The raw mass spectra were first extracted by Orbitool (Cai et al., 2020), and the molecular information was then achieved by applying a homemade toolkit based on MATLAB software. The toolkit drew on the idea from the "tofTools" package, which is used for analyzing the mass spectral data obtained from the TOF analyzer, such as a nitrate CI-API-TOF (Junninen et al., 2010). The concentrations of the detected species are then determined as follows:

$$[X] = \frac{i\left[X^-\right]}{NO_3^- \cdot (HNO_3)_{0\text{–}2}} \cdot C \quad (1)$$

where $i[X^-]$ is the transmission-corrected signal intensity of ion X in units of counts per second (cps) and C represents the calibration factor. C is determined from the collision frequency of target species with the nitrate ions (cluster) during its residence in the charger, taking into account the losses onto the walls of the reactor and the tube (Eq. 2):

$$C = C_{H_2SO_4} = \frac{1}{k_{ion} \cdot RT \cdot f_{inlet}}, \quad (2)$$

where k_{ions} is the ion collision frequency in the range of 1.7×10^{-9} to 2.3×10^{-9} cm^3 s^{-1} (Ehn et al., 2014), RT is the residence time in the charger and f_{inlet} represents the fractions of target species that passed through the inlet.

Herein, we apply the C determined for sulfuric acid (H_2SO_4) of 3.4×10^9 molecules cm^{-3} $ncps^{-1}$ to semi-quantify the concentrations of OOMs, which has been widely used in previous studies (Ehn et al., 2014; Yan et al., 2021; Yao et al., 2018). Among the low-volatility vapors, it has been demonstrated that nitrate ions exhibit the highest charging efficiency toward H_2SO_4 (Ehn et al., 2014; Hyttinen et al., 2015, 2018; Riva et al., 2019b). The estimated concentrations of OOMs thus can be considered the lower limits with an uncertainty of ±50 % according to error propagation (Ehn et al., 2014). Positive matrix factorization (PMF) was also performed for the measured species using Source Finder (SoFi, v6.3) based on Igor and run by the multilinear engine (ME-2) as detailed in Sect. S3 and Figs. S3–S6 (Canonaco et al., 2013).

3 Results and discussion

3.1 Chemical characteristics of OOMs

In total, we have identified 562 OOMs, which were concentrated in the carbon number (nC) range of 5 to 10, taking up 84.6 % of total OOMs during the whole campaign (unless otherwise stated, all the reported values hereafter correspond to the average of the whole campaign). Possible precursors of $C_{5–10}$ OOMs include isoprenes (C_5), benzene/alkylbenzenes ($C_{6–10}$), aliphatic VOCs ($C_{5–10}$) and monoterpenes (C_{10}) according to previous studies (Bianchi et al., 2019; Nie et al., 2022). $C_{\leq 4}$ OOMs only took up a small fraction of 6.7 % among total OOMs and were likely a result of the decomposition from OOMs with large carbon numbers as suggested by one of our companion studies (Zhang et al., 2022). The remaining 8.7 % were $C_{>10}$ OOMs, which accounted for a dominating fraction (70 %, Fig. S7) among the extremely low-volatility organic compounds (ELVOCs, $C^* < 3 \times 10^{-5}$ μg m^{-3}) based on a volatility parameterization proposed by Donahue and co-workers (Donahue et al., 2011, 2012; Schervish and Donahue, 2020) and potentially have larger impacts on SOA formation owing to their lower volatility.

We further classified the detected OOMs into four groups based on the number of N atoms they possessed, includ-

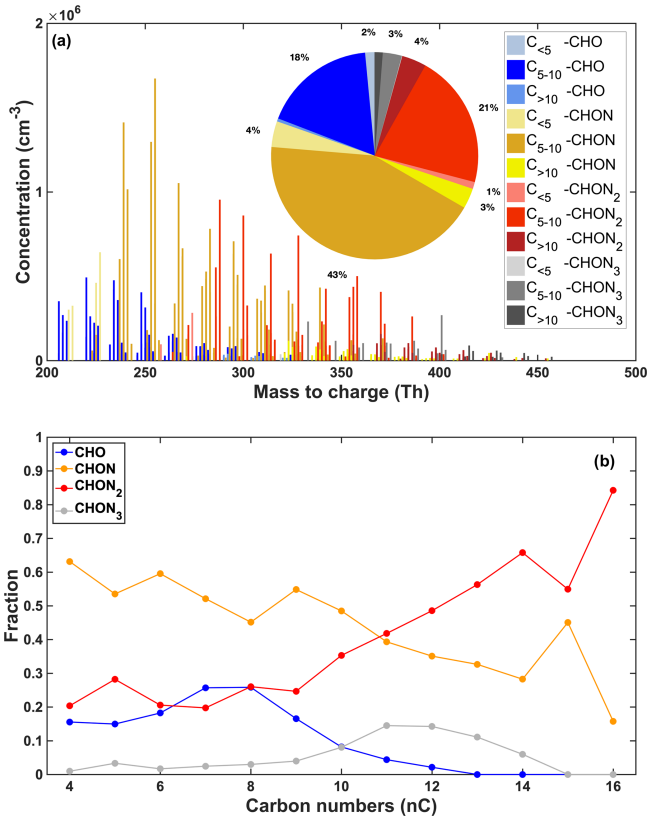

Figure 1. **(a)** Average mass spectrum of the detected OOMs during the whole campaign. The pie chart shows the fractions of OOMs with different numbers of nitrogen and carbon atoms; **(b)** the fractions of 0N-OOMs, 1N-OOMs, 2N-OOMs and 3N-OOMs among total OOMs as a function of the carbon number (nC).

ing non-nitrogen OOMs (0N-OOMs), 1N-OOMs, 2N-OOMs and 3N-OOMs. Their average fractional contributions to total OOM concentrations as well as the carbon number (nC) distributions are shown in Fig. 1. We found that 1N-OOMs dominated the total OOM concentration with an average fraction of 50 %, followed by 2N-OOMs (26 %), demonstrating the dominance of N-containing OOMs among total OOMs. The 3N-OOMs only took up a small fraction (4 %) of total OOMs, and the remaining 20 % were 0N-OOMs.

More interestingly, we found that 1N-OOMs prevailed among the OOMs with nC ≤ 10, yet 2N-OOMs dominated the $C_{>10}$ OOMs (41.8 %–84.2 %), suggesting the increased importance of multistep bimolecular oxidation in the formation of 2N-OOMs with nC > 10. We also note that the fraction of 2N-OOMs increased stepwise with the increase in nC (Fig. 1b), while 3N-OOMs did not exhibit a similar dependence. The potential reason for this is that, with the increase in nC on the one hand, more active sites are potentially provided to promote the occurrence of multistep oxidation, but on the other hand, the potentially larger steric effect can hinder multistep oxidation. From our observation, these two factors lead to an overall positive coupling for 2N-OOMs but result in a non-monotonic trend for 3N-OOMs. Furthermore, these 2N-OOMs with nC > 10 had an average molecular composition of $C_{12.5}H_{22.7}O_{2.1}(NO_3)_2$. Assuming the nitrogen atoms are only associated with the nitrate group ($-ONO_2$), the mean double-bond equivalent (DBE) value (Nie et al., 2022; Xu et al., 2021) was 1.15 on the carbon skeleton, suggesting its origination from aliphatic compounds, such as alkanes or alkenes (Gong et al., 2005; Mentel et al., 2015; Wang and Hildebrandt Ruiz, 2018).

We thus further classified the 2N-OOMs into their possible VOC precursors following a recently developed workflow proposed by Nie and co-workers, which is based on the up-to-date understanding of VOC oxidation and molecular characters (i.e., number of different elements, DBE) as well as PMF results (Nie et al., 2022), i.e., aromatics (2N-OOM$_{Aro}$), aliphatics (2N-OOM$_{Ali}$) and monoterpenes (2N-OOM$_{MT}$). Note that we classify isoprene 2N-OOMs (2N-OOM$_{Iso}$) as 2N-OOM$_{Ali}$ as well because of the low concentration of isoprene in the cold season. As a result, the average fractions of 2N-OOM$_{Aro}$, 2N-OOM$_{Ali}$ and 2N-OOM$_{MT}$ among total 2N-OOMs were 16.0 %, 64.2 % and 15.3 %, respectively (Fig. 2), suggesting significant contribution of aliphatic compounds to 2N-OOM formation. Taken together, the increased fraction of 2N-OOMs with the increase in nC and the dominant fraction of 2N-OOM$_{Ali}$ highlight the significant contribution of high-molecular-weight aliphatic precursors (i.e., intermediate-volatility or semi-volatile organic compounds, I/SVOCs) to high-molecular-weight 2N-OOM formation and comprise potentially important SOA material. We thus focus our attention on the formation of 2N-OOMs in the following sections.

3.2 2N-OOM formation in $PM_{2.5}$ episodes

To investigate the formation mechanisms and factors that may affect the 2N-OOM formation, 1 clean day (4–5 November) and 1 polluted day (7–8 November) based on the pollution levels, i.e., $PM_{2.5}$ concentrations, were selected for further analysis. Since OOM formation is directly mediated by photochemistry or nighttime chemistry, the clean and polluted cases were thus split into one clean daytime case (CL$_{day}$), one clean nighttime case (CL$_{night}$), one polluted daytime case (PL$_{day}$) and one polluted nighttime case (PL$_{night}$). Detailed information on durations, pollution levels, meteorological conditions and 2N-OOM concentrations during these four cases is summarized in Table 1.

During the whole campaign, the concentrations of 2N-OOMs ranged from 1.1×10^6 to 42.0×10^6 molecules cm^{-3} as shown in Fig. 2. We found the concentrations of 2N-OOMs in the polluted cases were 1.7–2.7 times higher than those in clean cases. Table 1 further indicates that the absolute abundances of almost all 2N-OOM classes were higher during the polluted cases as compared to the clean cases no matter whether it was the daytime or nighttime, except for the daytime 2N-OOM$_{Aro}$. Specifically, 2N-OOM$_{Ali}$ oc-

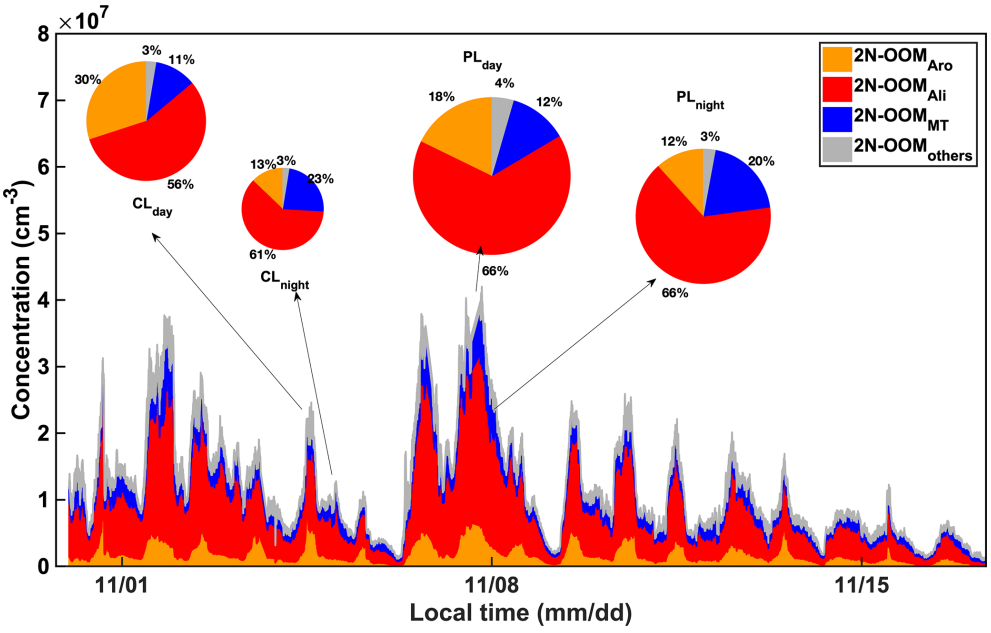

Figure 2. The time series of 2N-OOMs originating from different precursors. Four sub-periods were selected to further investigate the fractional distribution of different types of OOMs as shown in the pie charts, including a clean daytime case (12:00 to 14:00 LT on 4 November, $PM_{2.5} = 7.5\,\mu g\,m^{-3}$, CL_{day}), a clean nighttime case (23:00 LT on 4 November to 01:00 LT on 5 November, $PM_{2.5} = 9.5\,\mu g\,m^{-3}$, CL_{night}), a daytime case in a $PM_{2.5}$ episode (12:00 to 14:00 LT on 7 November, $PM_{2.5} = 44.0\,\mu g\,m^{-3}$, PL_{day}) and a nighttime case in a $PM_{2.5}$ episode (23:00 LT on 7 November to 01:00 LT on 8 November, $PM_{2.5} = 60.5\,\mu g\,m^{-3}$, PL_{night}). The sizes of pie charts are scaled to the total concentrations of 2N-OOMs.

cupied the largest fractions, which were even higher in polluted cases (66 %–66 %) than those in clean cases (56 %–61 %, Fig. 2). Especially for the 2N-OOM_{Ali} with nC > 10, its concentration in polluted cases increased by a factor of 2.3–4.8 compared to the clean cases (Fig. 3). From PMF analysis, we also identified a factor characterized by a series of 2N-OOM_{Ali} (i.e., $C_nH_{2n-2}O_8N_2$, $n = 5$ to 11) as the fingerprint molecules (Table S1). This factor tracks the $PM_{2.5}$ concentration well, especially during $PM_{2.5}$ episodes (Fig. S8), likely due to the availability of adequate aliphatic precursors during pollution episodes. Furthermore, 2N-OOM_{Ali} with nC > 10 presented both higher concentrations and higher fractions during daytime cases compared to nighttime cases (Fig. 3), suggesting that the photochemical formation of 2N-OOM_{Ali} prevailed compared to nighttime formation. To compare CL_{night} and PL_{night}, it was also found that the pollution case would lead to the enhanced importance of nighttime formation pathways of 2N-OOM_{Ali} with nC > 10.

We note that the fraction of 2N-OOM_{Ali} increased during CL_{night} primarily due to the more evident decrease in 2N-OOM_{Aro} (Table 1), whose formation is dominated by photochemistry. On the other hand, the decrease in 2N-OOM_{Aro} concentrations during PL_{night} was not as obvious as those during CL_{night}. Due to the significant increase in 2N-OOM_{Ali} concentration, the fraction of 2N-OOM_{Aro} species decreased in pollution cases, but their absolute concentrations only underwent a few changes in the daytime. The 2N-OOM_{MT} species showed significantly higher concentrations but similar fractions in polluted cases. On the other hand, equivalent or even slightly higher concentrations during the nighttime compared to those in the daytime suggest the comparable importance of nighttime chemistry in 2N-OOM_{MT} formation in contrast to 2N-OOM_{Ali} and 2N-OOM_{Aro}, which will be discussed in later subsections.

To summarize, the absolute concentrations of 2N-OOM were greatly affected by the pollution level for most cases. Both the concentrations and the fractions of 2N-OOM_{Ali} were significantly promoted by pollution conditions, whereas the 2N-OOM_{Aro} species were predominantly affected by photochemical production, whose formation was less sensitive to pollution levels compared to 2N-OOM_{Ali} in the daytime. In contrast, the absolute concentrations of 2N-OOM_{MT} were also significantly influenced by pollution levels but seem not solely dependent on the daytime/nighttime formation pathway. In addition, we note that both daytime photochemistry and nighttime chemistry had profound effects on 2N-OOM formation at different pollution levels, presumably depending on availability of the precursors as well as the oxidants. We thus focus our attention on the formation of 2N-OOMs during the daytime versus nighttime in the following sections.

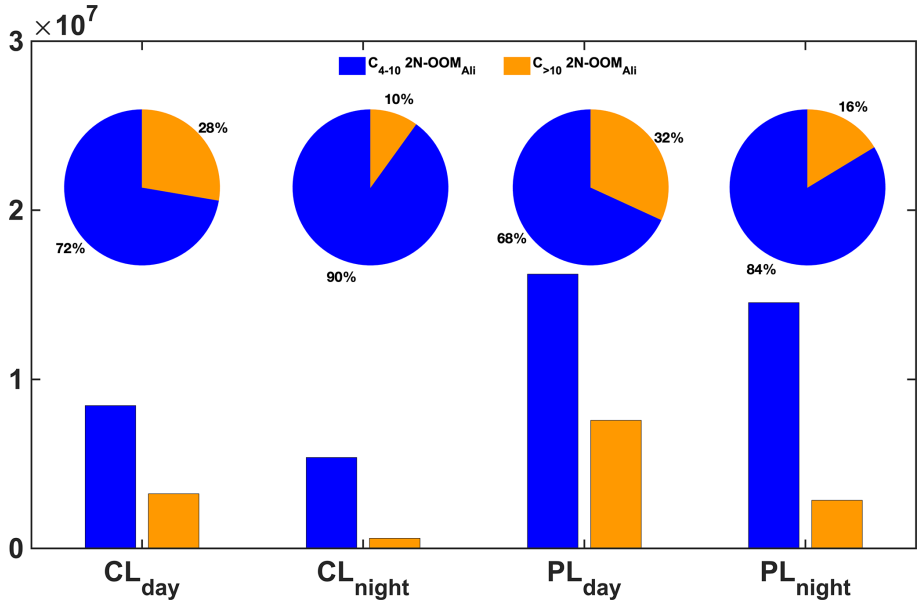

Figure 3. The fractions of 2N-OOM$_{Ali}$ with different carbon numbers in the four cases.

3.3 Daytime vs. nighttime formation of 2N-OOMs

We investigate the effects of photochemistry and nighttime chemistry on the formation of individual 2N-OOMs. While the former is dominated by OH radical oxidation, the latter involves NO_3 radical oxidation as well as reactions with ozone or other oxidants, e.g., halogen. Herein, we use solar radiation as a proxy for photochemical reactivity, and the concentrations of NO_3 radicals were estimated assuming that NO_3, NO_2 and N_2O_5 were under fast equilibration in the troposphere (Brown and Stutz, 2012). The correlation coefficients (Spearman type) between individual 2N-OOMs and solar radiation ($R_{2N\text{-}OOMs\text{-}solar}$) or NO_3 radicals ($R_{2N\text{-}OOMs\text{-}NO_3}$) derived from different precursors during the whole campaign are shown in Fig. 4a. It should be noted that the concentrations of 2N-OOMs and NO_3 radicals were scaled with the boundary layer height before calculating the correlation coefficients here and below for correcting the effects of meteorological dilution.

Both 2N-OOM$_{Aro}$ and 2N-OOM$_{Ali}$ showed stronger correlations with solar radiation compared to NO_3 radicals, indicating their association with daytime photochemistry, since benzene/alkylbenzenes and aliphatic VOCs rapidly react with OH radicals compared to other oxidants, such as NO_3 radicals. This is also supported by the observation that both 2N-OOM$_{Aro}$ and 2N-OOM$_{Ali}$ peaked during noontime (12:00–14:00 LT) as shown in Fig. 4b. Similarly, the PMF analysis also distinguished two daytime factors. The daytime factor 1 peaked at around 12:00–14:00 LT (Table S1) and highly correlated with solar radiation ($R = 0.57$). The fingerprint molecules of daytime factor 1 are $C_nH_{2n-4}O_{10}N_2$ ($n = 8$ to 10) with average DBE values of 2 on the carbon skeleton, suggesting the dominance of 2N-OOMs likely formed from aromatic precursors. Since each step of OH oxidation of aromatics followed by RO_2+NO_x termination would increase the hydrogen number (nH) by 1, this factor is likely dominated by 2N-OOMs formed from two steps of OH-initiated oxidation from alkylbenzenes given that the carbon numbers ranged from 8 to 10.

The key fingerprint molecule of daytime factor 2 is $C_nH_{2n}O_8N_2$ ($n = 4$ to 5) (accounting for 30.8 % in the factor profile), followed by $C_nH_{2n-2}O_8N_2$ ($n = 5$ to 6) (accounting for 9.7 % in the factor profile), which is likely a result of the decomposition from 2N-OOM$_{Ali}$ species with large carbon numbers, according to their DBE values of 0–1 on the carbon skeleton. This aliphatic factor presented even higher correlation with solar radiation ($R = 0.65$), peaking at around 12:00–14:00 LT. Strong daytime peaks together with the good correlations with irradiation suggest the dominance of photochemical oxidation in the formation of 2N-OOM$_{Ali}$. For 2N-OOM$_{Ali}$, although it showed strong a daytime peak, a weak nighttime peak was still observed. This indicates that although daytime formation of 2N-OOM$_{Ali}$ prevails, 2N-OOM$_{Ali}$ nighttime formation still existed. For example, we have obtained a nighttime factor from PMF analysis (nighttime factor 2), whose fingerprint molecules are $C_5H_8O_9N_2$ and $C_nH_{2n}O_7N_2$ ($n = 5$ to 8). $C_5H_8O_9N_2$ likely originated from isoprene, and $C_nH_{2n}O_7N_2$ was likely from anthropogenic aliphatic precursors.

Nighttime chemistry plays a more important role in the formation of 2N-OOM$_{MT}$. This is further supported by the slightly stronger correlation between 2N-OOM$_{MT}$ and NO_3 radicals compared to solar radiation. For some specific 2N-OOM$_{MT}$ species, the formation is likely a result of NO_3-radical-initiated oxidation. As shown in Fig. 5, we have iden-

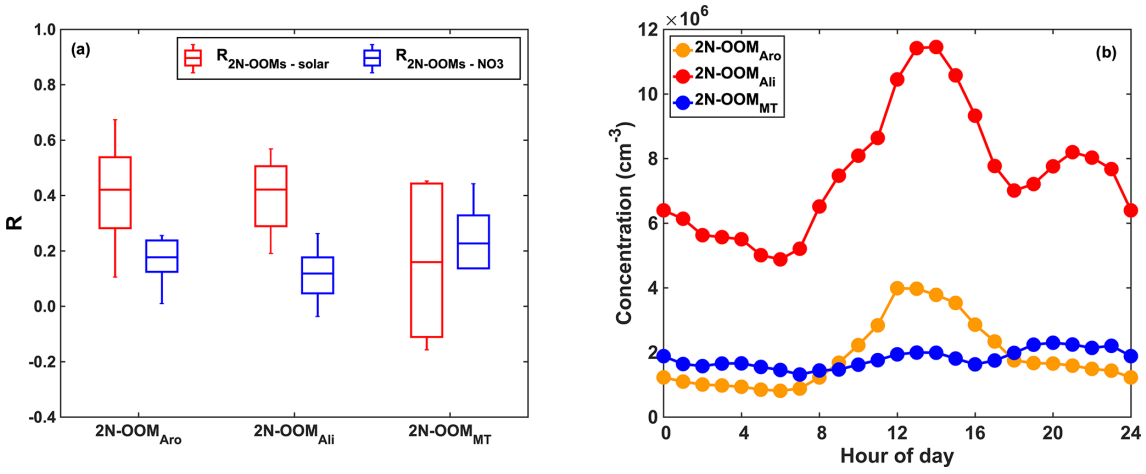

Figure 4. **(a)** Statistical distribution of the correlation coefficients (Spearman type) between 2N-OOMs and solar radiation ($R_{\text{2N-OOMs-solar}}$) in red and the correlation coefficients between 2N-OOMs and [NO_3] ($R_{\text{2N-OOMs-NO}_3}$) in blue for 2N-OOMs from different precursors. The horizontal lines are the median values, boxes denote the 25th- and 75th-percentile values, and whiskers represent the 10th- and 90th-percentile values. **(b)** The diel patterns of 2N-OOMs from different precursors.

tified a series of 2N-OOM_{MT} molecules with a molecular composition of $C_{10}H_{16}O_{7,9,11}N_2$, which showed strong positive correlations with NO_3 radicals. The occurrence of the propagation reaction from RO_2 to RO was critical to the formation of odd oxygen as proposed in previous chamber studies (Boyd et al., 2015; Claflin and Ziemann, 2018). Furthermore, under the nighttime conditions observed in urban Shanghai (Table 1), it is estimated that monoterpenes primarily react with NO_3, and the fate of nighttime RO_2's is dominated by NO, which is clearly different from rural environments where NO levels likely drop to near zero after sunset (Romer et al., 2016) and RO_2's are likely terminated by NO_3–RO_2 cross-reactions (Bates et al., 2022). Therefore, the formation of $C_{10}H_{16}O_{7,9,11}N_2$ likely started with the reaction of monoterpenes with NO_3 radicals forming a NO_3–$C_{10}H_{16}$ alkyl radical, followed by the formation of organic peroxy radicals (RO_2) upon addition of O_2. The RO_2 is then converted to an alkoxy radical (RO) upon reaction with NO. The autoxidation process would then start and introduce O_2 into the molecule stepwise, forming a series of more oxygenated RO_2 radicals, i.e., NO_3–$C_{10}H_{16}(O)(OO)_n$. The NO termination reaction of these RO_2 radicals would finally result in ONs with a chemical composition of NO_3–$C_{10}H_{16}(O)(OO)_nO(NO)O$ ($n = 0, 1, 2$).

On the other hand, the reaction rate between monoterpenes (i.e., α-pinene, β-pinene and limonene) and NO_3 is about 60 000–140 000 times faster than that between monoterpenes and O_3 at 293 K (Master Chemical Mechanism Version 3.3.1, MCMv3.3.1), but the averaged nighttime concentration of O_3 (22.8 ppb) was only about 18 000 times higher than that of NO_3 (1.3 ppt). Therefore, the NO_3-initiated oxidation process had significant impacts on 2N-OOM_{MT} formation during the nighttime. The 2N-OOM_{MT} resulting from NO_3 oxidation is also resolved as a nighttime factor (nighttime factor 1) from PMF analysis, which tracked the NO_3 concentrations well (Fig. S9, $R = 0.46$) and peaked at around 19:00–23:00 LT. The fingerprint molecule of nighttime factor 1 mainly included $C_{10}H_{16}O_9N_2$ and $C_{10}H_{16}O_8N_2$, which are generated from NO_3-initiated oxidation followed by NO termination, and this process will not change the nH of the parent monoterpene molecule.

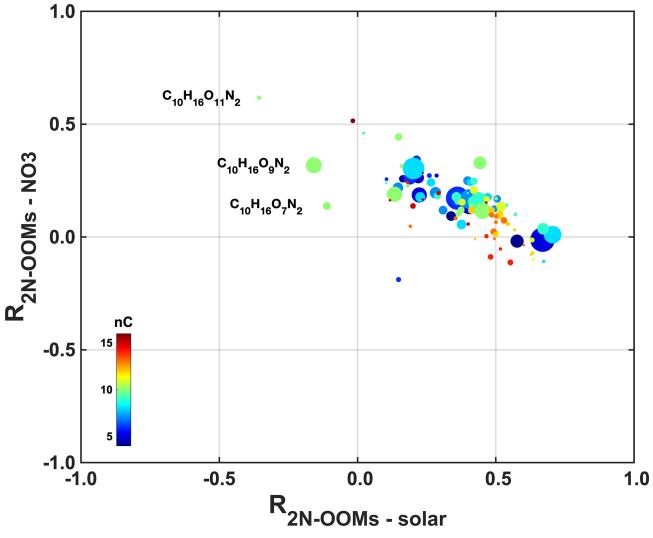

Figure 5. Scatterplot of $R_{\text{2N-OOMs-NO}_3}$ against $R_{\text{2N-OOMs-solar}}$ for specific 2N-OOM species.

3.4 Oxygenation level of 2N-OOMs

We then calculated the average effective oxygen number ($nO_{eff} = nO - 2nN$) of 2N-OOMs, which is used to indicate the oxidation state of carbon by excluding the oxygen atoms

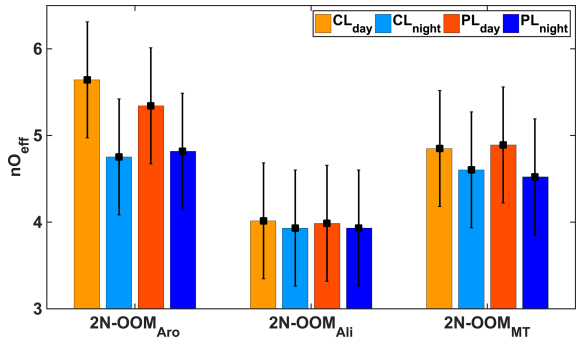

Figure 6. The nO_{eff} of 2N-OOMs derived from different precursors in the four cases; the error bars represent the standard deviations.

bonded with nitrogen atoms. Note that calculation of nO_{eff} assumes that the nitrogen atoms are only associated with the nitrate group ($-ONO_2$), which is reasonable after excluding nitrophenol peaks. The average nO_{eff} of 2N-OOMs from different precursors in CL_{day}, CL_{night}, PL_{day} and PL_{night} are shown in Fig. 6 and summarized in Table S2. The 2N-OOM_{Aro} had the highest nO_{eff} (4.8–5.6), followed by 2N-OOM_{MT} (4.5–4.9), and 2N-OOM_{Ali} had the lowest nO_{eff} (3.9–4.0). Difference in the oxygenation level of different types of OOMs can be attributed to the difference in oxidation mechanisms of the initiation reactions. For example, the OH-initiated oxidation of alkanes, aromatics and monoterpenes/alkenes would form a $C_xH_yO_2$ radical, $C_xH_yO_5$ radical and $C_xH_yO_3$ radical, respectively, incorporating different numbers of oxygen atoms into the original precursor molecules at the first step of oxidation (Master Chemical Mechanism Version 3.3.1, MCMv3.3.1). On the other hand, during the multiple-step oxidation in the daytime, aromatics could still provide more C=C bonds than other precursors after the initial step, which are plausibly capable of further reacting with OH, O_3 and other oxidants.

Furthermore, we also found that regardless of the pollution level, the nO_{eff} was considerably higher in daytime cases than in nighttime cases, particularly for 2N-OOM_{Aro} and 2N-OOM_{MT}, suggesting a profound effect of photochemistry on the formation of highly oxygenated 2N-OOMs. This is likely because of the high NO_x concentrations during the nighttime (Table 1), which could efficiently suppress the RO_2 radicals from autoxidation reactions, forming overall less oxygenated OOMs. The effect of NO_x on oxygenation levels will be discussed in a subsequent paragraph. The average nO_{eff} values of 2N-OOM_{Ali} in four sub-periods were similar without significant daytime and nighttime difference, ranging from 3.9–4.0. This could be partly explained by the fact that reactions with oxidants such as OH and halogen radicals will similarly result in the addition of oxygen atoms by 2 for alkanes during the first step of oxidation. Thus, the oxygenation levels of 2N-OOM_{Ali} were assumed to be insensitive to the oxidants in the daytime or nighttime.

Table 1. Summary of the four cases including the meteorological conditions and concentrations of trace gases and 2N-OOMs. Note that "ppt" denotes parts per trillion throughout this paper.

Case	Time (LT)	$PM_{2.5}$ ($\mu g\,m^{-3}$)	Solar ($W\,m^{-2}$)	T (°C)	RH (%)	$[O_3]$ (ppb)	$[NO]$ (ppb)	$[NO_2]$ (ppb)	$[NO_3]$ (ppt)	[2N-OOM_{Aro}] ($\times 10^6\,cm^{-3}$)	[2N-OOM_{Ali}] ($\times 10^6\,cm^{-3}$)	[2N-OOM_{MT}] ($\times 10^6\,cm^{-3}$)	[2N-OOM_{Total}] ($\times 10^6\,cm^{-3}$)
CL_{day}	4 November 12:00–14:00	7.5	635.6	18.9	35.2	41.9	3.2	8.2	0.1	6.3	11.7	2.3	20.8
CL_{night}	4 November 23:00–5 November 01:00	9.5	2.4	13.0	64.1	8.0	2.9	40.5	0.2	1.3	6.0	2.3	9.8
PL_{day}	7 November 12:00–14:00	44.0	384.5	23.9	30.5	73.9	2.2	20.6	0.3	6.4	23.8	4.3	36.2
PL_{night}	7 November 23:00–8 November 01:00	60.5	2.5	17.8	44.9	27.2	2.1	38.7	6.2	3.1	17.4	5.3	26.5

It is known that NO is also critical in determining the fate of RO_2 radicals during oxidation, forming RO radicals or organonitrates. Formation of RO radicals and of organonitrates will have opposite effects on the oxidation state of the termination products, since the former will significantly increase the oxygenation state of carbon through initiating propagation reactions before termination. We thus explore the effects of NO as well as the total NO_x concentrations on the average oxygenation levels of 2N-OOMs from different precursors during the whole campaign (Fig. 7). Consistently with previous studies in polluted urban environments (Qiao et al., 2021; Yan et al., 2021), the detected 2N-OOMs were also of low oxygenation with nO_{eff} values of 3.9–5.4 (25th–75th percentile) compared to those measured in forests or in laboratory studies (Berndt et al., 2016; Ehn et al., 2014; Jokinen et al., 2014; Rissanen et al., 2014; Yan et al., 2016). The nO_{eff} of 2N-OOM_{Aro} and 2N-OOM_{MT} increased with the decrease in NO or NO_x concentrations. This is likely due to the prevalence of NO termination reactions because the maximum autoxidation rate constant of alkylbenzenes with long-chain substituents (e.g., isopropylbenzene, ethylbenzene) and monoterpenes is comparable to the bimolecular reaction rate between RO_2 and NO (Bianchi et al., 2019). The oxygenation levels of 2N-OOM_{Ali} appear to be insensitive to the pollution levels and NO or NO_x concentrations, which should be further investigated in future studies.

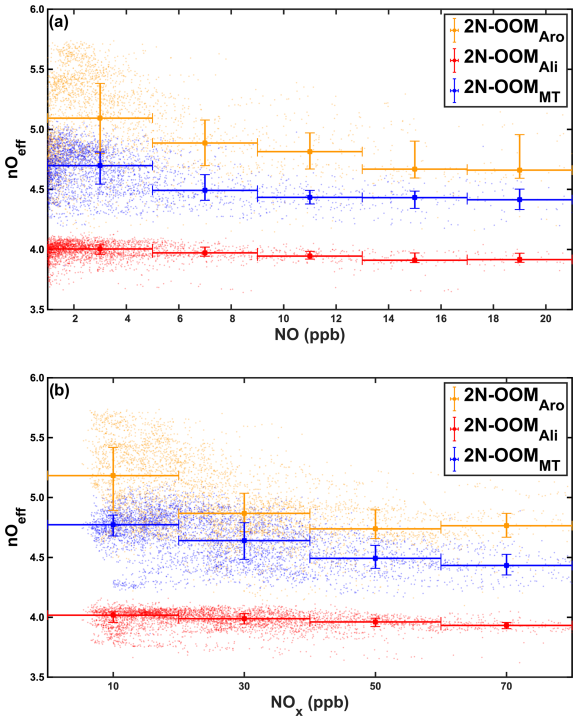

Figure 7. Effective oxygen number (nO_{eff}) of 2N-OOMs as a function of **(a)** NO concentration and **(b)** NO_x concentration. The colored squares represent the real measurements. The filled markers indicate the median values in the range as horizontal error bars show; the vertical error bars denote the 25th- and 75th-percentile values.

4 Conclusions

We report the unambiguous identification of 2N-OOMs as well as other OOMs using an ultra-high-resolution Orbitrap coupled with a nitrate inlet. We find that OOMs are distributed among a wide range of carbon numbers (nC = 4 to 16), among which the 2N-OOMs occupied a considerable fraction (26 %) of the total observed OOMs. During the whole campaign, the 2N-OOM concentrations ranged from 1.1×10^6 to 42.0×10^6 molecules cm^{-3} and were concentrated in the nC range of 5 to 10 with a high molecular weight (m/z > 350 Th), implying their low volatilities and thus potentially high contribution to local SOA formation.

Aliphatic, aromatics and monoterpenes were plausible precursors of 2N-OOMs with fractions of 64.2 %, 16 % and 15.4 %, respectively. The absolute concentrations of 2N-OOMs were greatly affected by the pollution level for most cases. The 2N-OOM_{Ali} was found to be the most abundant 2N-OOM, and its fraction even increased on the polluted day with an enhanced proportion of 2N-OOM_{Ali} species with nC > 10, probably due to the high concentrations of aliphatic precursors accompanied by $PM_{2.5}$ episodes. A significant contribution of long-chain aliphatic compounds (nC > 10) to 2N-OOM formation is also supported by the observation that the 2N-OOM fraction increased with the increase in nC and the species had low DBE values, likely through multistep bimolecular oxidation. The 2N-OOM_{Ali} and 2N-OOM_{Aro} mainly peaked in the daytime and showed stronger correlations with solar radiation over NO_3 radicals, indicating their association with daytime photochemistry, since benzene/alkylbenzenes and aliphatic hydrocarbons rapidly react with OH radicals compared with other oxidants, such as NO_3 radicals. In contrast, 2N-OOM_{MT} prevailed in both the daytime and the nighttime; some specific 2N-OOM_{MT} species showed strong positive correlations with NO_3 radicals and were likely a result of NO_3-radical-initiated oxidation, suggesting the comparable importance of nighttime NO_3 chemistry in 2N-OOM_{MT} formation. In terms of oxygenation levels, we found that 2N-OOM_{Aro} had the highest averaged nO_{eff} followed by 2N-OOM_{MT}. Daytime photochemistry and low NO_x concentrations had profound effects on the formation of more-oxygenated 2N-OOMs. The 2N-OOM_{Ali} had the lowest nO_{eff} and had negligible changes at different pollution levels. These results demonstrate the preference of 2N-OOM formation and the influencing factors in a Chinese megacity involving various VOC precursors (biogenic VOCs such as monoterpenes and anthropogenic VOCs such as aromatics and aliphatic hydrocarbons) and various atmospheric oxidants (such as OH radicals and NO_3 radicals) and highlight the influence of $PM_{2.5}$ episodes.

Data availability. Data presented in this paper are available upon request to the corresponding author.

Supplement. The supplement related to this article is available online at: https://doi.org/10.5194/acp-23-3233-2023-supplement.

Author contributions. CH designed this study. YL, YM, DDH, SL, SJ and YG conducted the field campaign. YL analyzed data with contributions from CH and all the other co-authors. YL wrote the manuscript with contributions from all the other co-authors.

Competing interests. The contact author has declared that none of the authors has any competing interests.

Disclaimer. Publisher's note: Copernicus Publications remains neutral with regard to jurisdictional claims in published maps and institutional affiliations.

Acknowledgements. This study was financially supported by the National Key Research and Development Program of China (2022YFC3700205) and China Postdoctoral Science Foundation (2022T150427, 2022M712146).

Financial support. This research has been supported by the National Key Research and Development Program of China (grant no. 2022YFC3700205) and the China Postdoctoral Science Foundation (grant nos. 2022T150427, 2022M712146).

Review statement. This paper was edited by Nga Lee Ng and reviewed by three anonymous referees.

References

Atkinson, R. and Arey, J.: Atmospheric Degradation of Volatile Organic Compounds, Chem. Rev., 103, 4605–4638, https://doi.org/10.1021/cr0206420, 2003.

Bates, K. H., Burke, G. J. P., Cope, J. D., and Nguyen, T. B.: Secondary organic aerosol and organic nitrogen yields from the nitrate radical (NO_3) oxidation of alpha-pinene from various RO_2 fates, Atmos. Chem. Phys., 22, 1467–1482, https://doi.org/10.5194/acp-22-1467-2022, 2022.

Berndt, T., Richters, S., Jokinen, T., Hyttinen, N., Kurtén, T., Otkjær, R. V., Kjaergaard, H. G., Stratmann, F., Herrmann, H., Sipilä, M., Kulmala, M., and Ehn, M.: Hydroxyl radical-induced formation of highly oxidized organic compounds, Nat. Commun., 7, 13677, https://doi.org/10.1038/ncomms13677, 2016.

Berndt, T., Scholz, W., Mentler, B., Fischer, L., Herrmann, H., Kulmala, M., and Hansel, A.: Accretion Product Formation from Self- and Cross-Reactions of RO_2 Radicals in the Atmosphere, Angew. Chem. Int. Ed., 57, 3820–3824, https://doi.org/10.1002/anie.201710989, 2018.

Bianchi, F., Kurtén, T., Riva, M., Mohr, C., Rissanen, M. P., Roldin, P., Berndt, T., Crounse, J. D., Wennberg, P. O., Mentel, T. F., Wildt, J., Junninen, H., Jokinen, T., Kulmala, M., Worsnop, D. R., Thornton, J. A., Donahue, N., Kjaergaard, H. G., and Ehn, M.: Highly Oxygenated Molecules (HOM) from Gas-Phase Autoxidation Involving Organic Peroxy Radicals: A Key Contributor to Atmospheric Aerosol, Chem. Rev., 119, 3472–3509, https://doi.org/10.1021/acs.chemrev.8b00395, 2019.

Boyd, C. M., Sanchez, J., Xu, L., Eugene, A. J., Nah, T., Tuet, W. Y., Guzman, M. I., and Ng, N. L.: Secondary organic aerosol formation from the β-pinene + NO_3 system: effect of humidity and peroxy radical fate, Atmos. Chem. Phys., 15, 7497–7522, https://doi.org/10.5194/acp-15-7497-2015, 2015.

Brown, S. S. and Stutz, J.: Nighttime radical observations and chemistry, Chem. Soc. Rev., 41, 6405–6447, https://doi.org/10.1039/c2cs35181a, 2012.

Cai, R., Li, Y., Clément, Y., Li, D., Dubois, C., Fabre, M., Besson, L., Perrier, S., George, C., Ehn, M., Huang, C., Yi, P., Ma, Y., and Riva, M.: Orbitool: a software tool for analyzing online Orbitrap mass spectrometry data, Atmos. Meas. Tech., 14, 2377–2387, https://doi.org/10.5194/amt-14-2377-2021, 2021.

Canonaco, F., Crippa, M., Slowik, J. G., Baltensperger, U., and Prévôt, A. S. H.: SoFi, an IGOR-based interface for the efficient use of the generalized multilinear engine (ME-2) for the source apportionment: ME-2 application to aerosol mass spectrometer data, Atmos. Meas. Tech., 6, 3649–3661, https://doi.org/10.5194/amt-6-3649-2013, 2013.

Claflin, M. S. and Ziemann, P. J.: Identification and Quantitation of Aerosol Products of the Reaction of β-Pinene with NO_3 Radicals and Implications for Gas- and Particle-Phase Reaction Mechanisms, J. Phys. Chem. A, 122, 3640–3652, https://doi.org/10.1021/acs.jpca.8b00692, 2018.

Ditto, J. C., Joo, T., Slade, J. H., Shepson, P. B., Ng, N. L., and Gentner, D. R.: Nontargeted Tandem Mass Spectrometry Analysis Reveals Diversity and Variability in Aerosol Functional Groups across Multiple Sites, Seasons, and Times of Day, Environ. Sci. Technol. Lett., 7, 60–69, https://doi.org/10.1021/acs.estlett.9b00702, 2020.

Donahue, N. M., Robinson, A. L., and Pandis, S. N.: Atmospheric organic particulate matter: From smoke to secondary organic aerosol, Atmos. Environ., 43, 94–106, https://doi.org/10.1016/j.atmosenv.2008.09.055, 2009.

Donahue, N. M., Epstein, S. A., Pandis, S. N., and Robinson, A. L.: A two-dimensional volatility basis set: 1. organic-aerosol mixing thermodynamics, Atmos. Chem. Phys., 11, 3303–3318, https://doi.org/10.5194/acp-11-3303-2011, 2011.

Donahue, N. M., Kroll, J. H., Pandis, S. N., and Robinson, A. L.: A two-dimensional volatility basis set – Part 2: Diagnostics of organic-aerosol evolution, Atmos. Chem. Phys., 12, 615–634, https://doi.org/10.5194/acp-12-615-2012, 2012.

Ehn, M., Thornton, J. A., Kleist, E., Sipilä, M., Junninen, H., Pullinen, I., Springer, M., Rubach, F., Tillmann, R., Lee, B., Lopez-Hilfiker, F., Andres, S., Acir, I.-H. H., Rissanen, M., Jokinen, T., Schobesberger, S., Kangasluoma, J., Kontkanen, J., Nieminen, T., Kurtén, T., Nielsen, L. B., Jørgensen, S., Kjaergaard, H. G., Canagaratna, M., Maso, M. D., Berndt, T., Petäjä, T., Wahner, A., Kerminen, V.-M. M., Kulmala, M., Worsnop,

D. R., Wildt, J., and Mentel, T. F.: A large source of low-volatility secondary organic aerosol, Nature, 506, 476–479, https://doi.org/10.1038/nature13032, 2014.

Garmash, O., Rissanen, M. P., Pullinen, I., Schmitt, S., Kausiala, O., Tillmann, R., Zhao, D., Percival, C., Bannan, T. J., Priestley, M., Hallquist, Å. M., Kleist, E., Kiendler-Scharr, A., Hallquist, M., Berndt, T., McFiggans, G., Wildt, J., Mentel, T. F., and Ehn, M.: Multi-generation OH oxidation as a source for highly oxygenated organic molecules from aromatics, Atmos. Chem. Phys., 20, 515–537, https://doi.org/10.5194/acp-20-515-2020, 2020.

Gong, H., Matsunaga, A., and Ziemann, P. J.: Products and mechanism of secondary organic aerosol formation from reactions of linear alkenes with NO_3 Radicals, J. Phys. Chem. A, 109, 4312–4324, https://doi.org/10.1021/jp058024l, 2005.

Hallquist, M., Wenger, J. C., Baltensperger, U., Rudich, Y., Simpson, D., Claeys, M., Dommen, J., Donahue, N. M., George, C., Goldstein, A. H., Hamilton, J. F., Herrmann, H., Hoffmann, T., Iinuma, Y., Jang, M., Jenkin, M. E., Jimenez, J. L., Kiendler-Scharr, A., Maenhaut, W., McFiggans, G., Mentel, Th. F., Monod, A., Prévôt, A. S. H., Seinfeld, J. H., Surratt, J. D., Szmigielski, R., and Wildt, J.: The formation, properties and impact of secondary organic aerosol: current and emerging issues, Atmos. Chem. Phys., 9, 5155–5236, https://doi.org/10.5194/acp-9-5155-2009, 2009.

Heinritzi, M., Simon, M., Steiner, G., Wagner, A. C., Kürten, A., Hansel, A., and Curtius, J.: Characterization of the mass-dependent transmission efficiency of a CIMS, Atmos. Meas. Tech., 9, 1449–1460, https://doi.org/10.5194/amt-9-1449-2016, 2016.

Hyttinen, N., Kupiainen-Määttä, O., Rissanen, M. P., Muuronen, M., Ehn, M., and Kurtén, T.: Modeling the Charging of Highly Oxidized Cyclohexene Ozonolysis Products Using Nitrate-Based Chemical Ionization, J. Phys. Chem. A, 119, 6339–6345, https://doi.org/10.1021/acs.jpca.5b01818, 2015.

Hyttinen, N., Otkjær, R. V., Iyer, S., Kjaergaard, H. G., Rissanen, M. P., Wennberg, P. O., and Kurtén, T.: Computational Comparison of Different Reagent Ions in the Chemical Ionization of Oxidized Multifunctional Compounds, J. Phys. Chem. A, 122, 269–279, https://doi.org/10.1021/acs.jpca.7b10015, 2018.

Jimenez, J. L., Canagaratna, M. R., Donahue, N. M., Prevot, A. S. H. H., Zhang, Q., Kroll, J. H., DeCarlo, P. F., Allan, J. D., Coe, H., Ng, N. L., Aiken, A. C., Docherty, K. S., Ulbrich, I. M., Grieshop, A. P., Robinson, A. L., Duplissy, J., Smith, J. D., Wilson, K. R., Lanz, V. A., Hueglin, C., Sun, Y. L., Tian, J., Laaksonen, A., Raatikainen, T., Rautiainen, J., Vaattovaara, P., Ehn, M., Kulmala, M., Tomlinson, J. M., Collins, D. R., Cubison, M. J., Dunlea, J., Huffman, J. A., Onasch, T. B., Alfarra, M. R., Williams, P. I., Bower, K., Kondo, Y., Schneider, J., Drewnick, F., Borrmann, S., Weimer, S., Demerjian, K., Salcedo, D., Cottrell, L., Griffin, R., Takami, A., Miyoshi, T., Hatakeyama, S., Shimono, A., Sun, J. Y., Zhang, Y. M., Dzepina, K., Kimmel, J. R., Sueper, D., Jayne, J. T., Herndon, S. C., Trimborn, A. M., Williams, L. R., Wood, E. C., Middlebrook, A. M., Kolb, C. E., Baltensperger, U., Worsnop, D. R., Dunlea, E. J., Huffman, J. A., Onasch, T. B., Alfarra, M. R., Williams, P. I., Bower, K., Kondo, Y., Schneider, J., Drewnick, F., Borrmann, S., Weimer, S., Demerjian, K., Salcedo, D., Cottrell, L., Griffin, R., Takami, A., Miyoshi, T., Hatakeyama, S., Shimono, A., Sun, J. Y., Zhang, Y. M., Dzepina, K., Kimmel, J. R., Sueper, D., Jayne, J. T., Herndon, S. C., Trimborn, A. M., Williams, L. R., Wood, E. C., Middlebrook, A. M., Kolb, C. E., Baltensperger, U., and Worsnop, D. R.: Evolution of Organic Aerosols in the Atmosphere, Science, 326, 1525–1529, https://doi.org/10.1126/science.1180353, 2009.

Jokinen, T., Sipilä, M., Richters, S., Kerminen, V. M., Paasonen, P., Stratmann, F., Worsnop, D., Kulmala, M., Ehn, M., Herrmann, H., and Berndt, T.: Rapid autoxidation forms highly oxidized RO_2 radicals in the atmosphere, Angew. Chemie Int. Ed., 53, 14596–14600, https://doi.org/10.1002/anie.201408566, 2014.

Jokinen, T., Berndt, T., Makkonen, R., Kerminen, V.-M., Junninen, H., Paasonen, P., Stratmann, F., Herrmann, H., Guenther, A. B., Worsnop, D. R., Kulmala, M., Ehn, M., and Sipilä, M.: Production of extremely low volatile organic compounds from biogenic emissions: Measured yields and atmospheric implications, P. Natl. Acad. Sci. USA, 112, 7123–7128, https://doi.org/10.1073/pnas.1423977112, 2015.

Junninen, H., Ehn, M., Petäjä, T., Luosujärvi, L., Kotiaho, T., Kostiainen, R., Rohner, U., Gonin, M., Fuhrer, K., Kulmala, M., and Worsnop, D. R.: A high-resolution mass spectrometer to measure atmospheric ion composition, Atmos. Meas. Tech., 3, 1039–1053, https://doi.org/10.5194/amt-3-1039-2010, 2010.

Kenagy, H. S., Present, P. S. R., Wooldridge, P. J., Nault, B. A., Campuzano-jost, P., Day, D. A., Jimenez, J. L., Zare, A., Pye, H. O. T., Yu, J., Song, C. H., Blake, D. R., Woo, J., Kim, Y., and Cohen, R. C.: Contribution of Organic Nitrates to Organic Aerosol over South Korea during KORUS-AQ, Environ. Sci. Technol., 55, 16326–16338, https://doi.org/10.1021/acs.est.1c05521, 2021.

Kiendler-Scharr, A., Mensah, A. A., Friese, E., Topping, D., Nemitz, E., Prevot, A. S. H., Äijälä, M., Allan, J., Canonaco, F., Canagaratna, M., Carbone, S., Crippa, M., Dall Osto, M., Day, D. A., De Carlo, P., Di Marco, C. F., Elbern, H., Eriksson, A., Freney, E., Hao, L., Herrmann, H., Hildebrandt, L., Hillamo, R., Jimenez, J. L., Laaksonen, A., McFiggans, G., Mohr, C., O'Dowd, C., Otjes, R., Ovadnevaite, J., Pandis, S. N., Poulain, L., Schlag, P., Sellegri, K., Swietlicki, E., Tiitta, P., Vermeulen, A., Wahner, A., Worsnop, D., and Wu, H. C.: Ubiquity of organic nitrates from nighttime chemistry in the European submicron aerosol, Geophys. Res. Lett., 43, 7735–7744, https://doi.org/10.1002/2016GL069239, 2016.

Lee, B. H., Mohr, C., Lopez-Hilfiker, F. D., Lutz, A., Hallquist, M., Lee, L., Romer, P., Cohen, R. C., Iyer, S., Kurtén, T., Hu, W., Day, D. A., Campuzano-Jost, P., Jimenez, J. L., Xu, L., Ng, N. L., Guo, H., Weber, R. J., Wild, R. J., Brown, S. S., Koss, A., De Gouw, J., Olson, K., Goldstein, A. H., Seco, R., Kim, S., McAvey, K., Shepson, P. B., Starn, T., Baumann, K., Edgerton, E. S., Liu, J., Shilling, J. E., Miller, D. O., Brune, W., Schobesberger, S., D'Ambro, E. L., and Thornton, J. A.: Highly functionalized organic nitrates in the southeast United States: Contribution to secondary organic aerosol and reactive nitrogen budgets, P. Natl. Acad. Sci. USA, 113, 1516–1521, https://doi.org/10.1073/pnas.1508108113, 2016.

Liebmann, J., Sobanski, N., Schuladen, J., Karu, E., Hellén, H., Hakola, H., Zha, Q., Ehn, M., Riva, M., Heikkinen, L., Williams, J., Fischer, H., Lelieveld, J., and Crowley, J. N.: Alkyl nitrates in the boreal forest: formation via the NO_3-, OH- and O_3-induced oxidation of biogenic volatile organic compounds and ambient lifetimes, Atmos. Chem. Phys., 19, 10391–10403, https://doi.org/10.5194/acp-19-10391-2019, 2019.

Lin, C., Huang, R. J., Duan, J., Zhong, H., and Xu, W.: Primary and Secondary Organic Nitrate in Northwest China: A Case Study, Environ. Sci. Technol. Lett., 8, 947–953, https://doi.org/10.1021/acs.estlett.1c00692, 2021.

Mentel, T. F., Springer, M., Ehn, M., Kleist, E., Pullinen, I., Kurtén, T., Rissanen, M., Wahner, A., and Wildt, J.: Formation of highly oxidized multifunctional compounds: autoxidation of peroxy radicals formed in the ozonolysis of alkenes – deduced from structure–product relationships, Atmos. Chem. Phys., 15, 6745–6765, https://doi.org/10.5194/acp-15-6745-2015, 2015.

Ng, N. L., Brown, S. S., Archibald, A. T., Atlas, E., Cohen, R. C., Crowley, J. N., Day, D. A., Donahue, N. M., Fry, J. L., Fuchs, H., Griffin, R. J., Guzman, M. I., Herrmann, H., Hodzic, A., Iinuma, Y., Jimenez, J. L., Kiendler-Scharr, A., Lee, B. H., Luecken, D. J., Mao, J., McLaren, R., Mutzel, A., Osthoff, H. D., Ouyang, B., Picquet-Varrault, B., Platt, U., Pye, H. O. T., Rudich, Y., Schwantes, R. H., Shiraiwa, M., Stutz, J., Thornton, J. A., Tilgner, A., Williams, B. J., and Zaveri, R. A.: Nitrate radicals and biogenic volatile organic compounds: oxidation, mechanisms, and organic aerosol, Atmos. Chem. Phys., 17, 2103–2162, https://doi.org/10.5194/acp-17-2103-2017, 2017.

Nie, W., Yan, C., Huang, D. D., Wang, Z., Liu, Y., Qiao, X., Guo, Y., Tian, L., Zheng, P., Xu, Z., Li, Y., Xu, Z., Qi, X., Sun, P., Wang, J., Zheng, F., Li, X., Yin, R., Dallenbach, K. R., Bianchi, F., Petäjä, T., Zhang, Y., Wang, M., Schervish, M., Wang, S., Qiao, L., Wang, Q., Zhou, M., Wang, H., Yu, C., Yao, D., Guo, H., Ye, P., Lee, S., Li, Y. J., Liu, Y., Chi, X., Kerminen, V.-M., Ehn, M., Donahue, N. M., Wang, T., Huang, C., Kulmala, M., Worsnop, D., Jiang, J., and Ding, A.: Secondary organic aerosol formed by condensing anthropogenic vapours over China's megacities, Nat. Geosci., 15, 255–261, https://doi.org/10.1038/s41561-022-00922-5, 2022.

Pye, H. O. T., D'Ambro, E. L., Lee, B. H., Schobesberger, S., Takeuchi, M., Zhao, Y., Lopez-Hilfiker, F., Liu, J., Shilling, J. E., Xing, J., Mathur, R., Middlebrook, A. M., Liao, J., Welti, A., Graus, M., Warneke, C., de Gouw, J. A., Holloway, J. S., Ryerson, T. B., Pollack, I. B., and Thornton, J. A.: Anthropogenic enhancements to production of highly oxygenated molecules from autoxidation, P. Natl. Acad. Sci. USA, 116, 6641–6646, https://doi.org/10.1073/pnas.1810774116, 2019.

Qiao, X., Yan, C., Li, X., Guo, Y., Yin, R., Deng, C., Li, C., Nie, W., Wang, M., Cai, R., Huang, D., Wang, Z., Yao, L., Worsnop, D. R., Bianchi, F., Liu, Y., Donahue, N. M., Kulmala, M., and Jiang, J.: Contribution of Atmospheric Oxygenated Organic Compounds to Particle Growth in an Urban Environment, Environ. Sci. Technol., 55, 13646–13656, https://doi.org/10.1021/acs.est.1c02095, 2021.

Rissanen, M. P., Kurtén, T., Sipilä, M., Thornton, J. A., Kangasluoma, J., Sarnela, N., Junninen, H., Jørgensen, S., Schallhart, S., Kajos, M. K., Taipale, R., Springer, M., Mentel, T. F., Ruuskanen, T., Petäjä, T., Worsnop, D. R., Kjaergaard, H. G., and Ehn, M.: The formation of highly oxidized multifunctional products in the ozonolysis of cyclohexene, J. Am. Chem. Soc., 136, 15596–15606, https://doi.org/10.1021/ja507146s, 2014.

Riva, M.: Multiphase Chemistry of Highly Oxidized Molecules: The Case of Organic Hydroperoxides, Chem, 1, 526–528, https://doi.org/10.1016/j.chempr.2016.09.015, 2016.

Riva, M., Ehn, M., Li, D., Tomaz, S., Bourgain, F., Perrier, S., and George, C.: CI-Orbitrap: An Analytical Instrument to Study Atmospheric Reactive Organic Species, Anal. Chem., 91, 9419–9423, https://doi.org/10.1021/acs.analchem.9b02093, 2019a.

Riva, M., Rantala, P., Krechmer, J. E., Peräkylä, O., Zhang, Y., Heikkinen, L., Garmash, O., Yan, C., Kulmala, M., Worsnop, D., and Ehn, M.: Evaluating the performance of five different chemical ionization techniques for detecting gaseous oxygenated organic species, Atmos. Meas. Tech., 12, 2403–2421, https://doi.org/10.5194/amt-12-2403-2019, 2019b.

Rollins, A. W., Pusede, S., Wooldridge, P., Min, K. E., Gentner, D. R., Goldstein, A. H., Liu, S., Day, D. A., Russell, L. M., Rubitschun, C. L., Surratt, J. D., and Cohen, R. C.: Gas/particle partitioning of total alkyl nitrates observed with TD-LIF in Bakersfield, J. Geophys. Res.-Atmos., 118, 6651–6662, https://doi.org/10.1002/jgrd.50522, 2013.

Romer, P. S., Duffey, K. C., Wooldridge, P. J., Allen, H. M., Ayres, B. R., Brown, S. S., Brune, W. H., Crounse, J. D., de Gouw, J., Draper, D. C., Feiner, P. A., Fry, J. L., Goldstein, A. H., Koss, A., Misztal, P. K., Nguyen, T. B., Olson, K., Teng, A. P., Wennberg, P. O., Wild, R. J., Zhang, L., and Cohen, R. C.: The lifetime of nitrogen oxides in an isoprene-dominated forest, Atmos. Chem. Phys., 16, 7623–7637, https://doi.org/10.5194/acp-16-7623-2016, 2016.

Schervish, M. and Donahue, N. M.: Peroxy radical chemistry and the volatility basis set, Atmos. Chem. Phys., 20, 1183–1199, https://doi.org/10.5194/acp-20-1183-2020, 2020.

Wang, D. S. and Hildebrandt Ruiz, L.: Chlorine-initiated oxidation of n-alkanes under high-NO_x conditions: insights into secondary organic aerosol composition and volatility using a FIGAERO–CIMS, Atmos. Chem. Phys., 18, 15535–15553, https://doi.org/10.5194/acp-18-15535-2018, 2018.

Wang, Y., Mehra, A., Krechmer, J. E., Yang, G., Hu, X., Lu, Y., Lambe, A., Canagaratna, M., Chen, J., Worsnop, D., Coe, H., and Wang, L.: Oxygenated products formed from OH-initiated reactions of trimethylbenzene: autoxidation and accretion, Atmos. Chem. Phys., 20, 9563–9579, https://doi.org/10.5194/acp-20-9563-2020, 2020.

Xu, L., Suresh, S., Guo, H., Weber, R. J., and Ng, N. L.: Aerosol characterization over the southeastern United States using high-resolution aerosol mass spectrometry: spatial and seasonal variation of aerosol composition and sources with a focus on organic nitrates, Atmos. Chem. Phys., 15, 7307–7336, https://doi.org/10.5194/acp-15-7307-2015, 2015.

Xu, Z. N., Nie, W., Liu, Y. L., Sun, P., Huang, D. D., Yan, C., Krechmer, J., Ye, P. L., Xu, Z., Qi, X. M., Zhu, C. J., Li, Y. Y., Wang, T. Y., Wang, L., Huang, X., Tang, R. Z., Guo, S., Xiu, G. L., Fu, Q. Y., Worsnop, D., Chi, X. G., and Ding, A. J.: Multifunctional Products of Isoprene Oxidation in Polluted Atmosphere and Their Contribution to SOA, Geophys. Res. Lett., 48, 1–10, https://doi.org/10.1029/2020GL089276, 2021.

Yan, C., Nie, W., Äijälä, M., Rissanen, M. P., Canagaratna, M. R., Massoli, P., Junninen, H., Jokinen, T., Sarnela, N., Häme, S. A. K., Schobesberger, S., Canonaco, F., Yao, L., Prévôt, A. S. H., Petäjä, T., Kulmala, M., Sipilä, M., Worsnop, D. R., and Ehn, M.: Source characterization of highly oxidized multifunctional compounds in a boreal forest environment using positive matrix factorization, Atmos. Chem. Phys., 16, 12715–12731, https://doi.org/10.5194/acp-16-12715-2016, 2016.

Yan, C., Yin, R., Lu, Y., Dada, L., Yang, D., Fu, Y., Kontkanen, J., Deng, C., Garmash, O., Ruan, J., Baalbaki, R., Schervish,

M., Cai, R., Bloss, M., Chan, T., Chen, T., Chen, Q., Chen, X., Chen, Y., Chu, B., Dällenbach, K., Foreback, B., He, X., Heikkinen, L., Jokinen, T., Junninen, H., Kangasluoma, J., Kokkonen, T., Kurppa, M., Lehtipalo, K., Li, H., Li, H., Li, X., Liu, Y., Ma, Q., Paasonen, P., Rantala, P., Pileci, R. E., Rusanen, A., Sarnela, N., Simonen, P., Wang, S., Wang, W., Wang, Y., Xue, M., Yang, G., Yao, L., Zhou, Y., Kujansuu, J., Petäjä, T., Nie, W., Ma, Y., Ge, M., He, H., Donahue, N. M., Worsnop, D. R., Veli-Matti Kerminen, Wang, L., Liu, Y., Zheng, J., Kulmala, M., Jiang, J., and Bianchi, F.: The Synergistic Role of Sulfuric Acid, Bases, and Oxidized Organics Governing New-Particle Formation in Beijing, Geophys. Res. Lett., 48, 2020GL091944, https://doi.org/10.1029/2020gl091944, 2021.

Yao, L., Garmash, O., Bianchi, F., Zheng, J., Yan, C., Kontkanen, J., Junninen, H., Mazon, S. B., Ehn, M., Paasonen, P., Sipilä, M., Wang, M., Wang, X., Xiao, S., Chen, H., Lu, Y., Zhang, B., Wang, D., Fu, Q., Geng, F., Li, L., Wang, H., Qiao, L., Yang, X., Chen, J., Kerminen, V.-M., Petäjä, T., Worsnop, D. R., Kulmala, M., and Wang, L.: Atmospheric new particle formation from sulfuric acid and amines in a Chinese megacity, Science, 361, 278–281, https://doi.org/10.1126/science.aao4839, 2018.

Ye, C., Yuan, B., Lin, Y., Wang, Z., Hu, W., Li, T., Chen, W., Wu, C., Wang, C., Huang, S., Qi, J., Wang, B., Wang, C., Song, W., Wang, X., Zheng, E., Krechmer, J. E., Ye, P., Zhang, Z., Wang, X., Worsnop, D. R., and Shao, M.: Chemical characterization of oxygenated organic compounds in the gas phase and particle phase using iodide CIMS with FIGAERO in urban air, Atmos. Chem. Phys., 21, 8455–8478, https://doi.org/10.5194/acp-21-8455-2021, 2021.

Yu, K., Zhu, Q., Du, K., and Huang, X.-F.: Characterization of nighttime formation of particulate organic nitrates based on high-resolution aerosol mass spectrometry in an urban atmosphere in China, Atmos. Chem. Phys., 19, 5235–5249, https://doi.org/10.5194/acp-19-5235-2019, 2019.

Zhang, Y., Li, D., Ma, Y., Dubois, C., Wang, X., Perrier, S., Chen, H., Wang, H., Jing, S., Lu, Y., Lou, S., Yan, C., Nie, W., Chen, J., Huang, C., George, C., and Riva, M.: Field Detection of Highly Oxygenated Organic Molecules in Shanghai by Chemical Ionization–Orbitrap, Environ. Sci. Technol., 56, 7608–7617, https://doi.org/10.1021/acs.est.1c08346, 2022.

Zhao, Y., Thornton, J. A., and Pye, H. O. T.: Quantitative constraints on autoxidation and dimer formation from direct probing of monoterpene-derived peroxy radical chemistry, P. Natl. Acad. Sci. USA, 115, 12142–12147, https://doi.org/10.1073/pnas.1812147115, 2018.